Control Engineering Practice 133 (2023) 105452

Contents lists available at ScienceDirect

Control Engineering Practice

journal homepage: www.elsevier.com/locate/conengprac

Cooperative control and stability analysis for virtual coupling of rail vehicles

Dario Bauso [a,b,*], Claudia Fecarotti [c], Azin Khaleghi [a]

[a] Jan C. Willems Center for Systems and Control, ENTEG, University of Groningen, Nijenborgh 4, 9747 AG Groningen, The Netherlands
[b] Dipartimento di Ingegneria, Università di Palermo, 90128 Palermo, Italy
[c] Department of Industrial Engineering & Innovation Sciences, Operations Planning Accounting & Control Group, Eindhoven University of Technology, School of Industrial Engineering, P.O. Box 513, 5600 MB Eindhoven, The Netherlands

ARTICLE INFO

MSC:
93-XX

Keywords:
Cooperative control
Consensus
Autonomous vehicles

ABSTRACT

Cooperative control for rail vehicles is a new idea which builds on existing models and methods developed in the context of flight formation and autonomous ground vehicles. The underlying idea is to assimilate virtually coupled rail vehicles to arrays of mass–spring–dashpot systems. The contribution of this paper is three-fold. First, a novel scheme is proposed which involves a supervisory control for the higher-level planning and a local motion coordination for the lower-level implementation. For the supervisory control, a review of the existing scheduling models and methods based on alternate graphs and a mixed-integer (non)linear program is conducted. For the local coordination, a nonlinear and uncertain model is developed and a constructive method is provided to design a feedback control that stabilizes the vehicle around a desired equilibrium point, in terms of position and velocity. Second, the control design method is extended to the case of multiple virtually coupled vehicles. It is proven that the transient dynamics follows a typical synchronization dynamics. It is also proven that under such control, the whole system of rail vehicles converges to a pre-defined equilibrium point, characterized by a specific velocity and relative distance between vehicles. Conditions for the stability of such equilibrium points are investigated. Third, under the hypothesis of homogeneity, bounds on the damping coefficient for the synchronization equilibrium (in terms of velocity and relative distance between vehicles) to be overdamped or underdamped are provided.

1. Introduction

Due to the rising traffic demands, autonomous trains will play a crucial role in the future of transportation systems in terms of safety, efficiency, and accessibility. However, an increased level of automation brings new challenges in the scheduling and coordination of the train vehicles, especially in response to unforeseen events which affect the timetable of the trains (Bersani et al., 2015). Within this context, a methodological approach involving supervisory control and local coordination control is proposed. The proposed approach contributes to advancing models and methods within the ERTMS.

The study of network robustness as a concept to tackle expected and unexpected disturbances and estimate the stability and efficiency of railway traffic is the main focus in Friedrich et al. (2018), Jiao et al. (2020), Lusby et al. (2018). Likewise, in this paper, a robust control method is proposed that guarantees the stability properties of the control method under dynamic and uncertain parameters within certain bounds.

Cooperative control for rail vehicles (Dong et al., 2016; Shamma, 2008; Xun et al., 2013, 2019; Yin et al., 2017) deals with building mathematical models based on the mechanical analogue according to which trains are convoys of autonomous and mobile unit components virtually coupled via a spring and a dashpot. Within the literature on cooperative control, a control design is developed in Su et al. (2021), in which the energy consumption is minimized by optimizing the operation of the trains. In Gao et al. (2013), a decentralized cooperative control approach is used in order to address the coordination problem with the heavy-haul trains. The idea of assimilating autonomous vehicles to arrays of mass–spring–dashpot systems is well established in other sectors such as consensus (Olfati-Saber & Murray, 2004; Ren, 2007; Ren et al., 2005), coupled oscillators (Yin et al., 2011, 2014), swarms (Liu & Passino, 2004), autonomous vehicles (Dunbar & Murray, 2006; Fax & Murray, 2004; Santini et al., 2016) or UAVs flight formation (Bauso et al., 2006; Giulietti et al., 2000). The idea of virtual coupling builds on communication-based train control systems (Ning et al., 2014; Wang et al., 2015; Zhu et al., 2014). Within the literature on autonomous vehicles, the authors in Jadbabaie et al. (2003) investigate consensus on headings of n different autonomous agents. In Olfati-Saber et al. (2007), the authors analyze consensus algorithms and their applications to networked systems. A consensus algorithm is extended to second-ordered dynamic systems and applied to formation

* Corresponding author at: Jan C. Willems Center for Systems and Control, ENTEG, University of Groningen, Nijenborgh 4, 9747 AG Groningen, The Netherlands.
E-mail address: d.bauso@rug.nl (D. Bauso).

https://doi.org/10.1016/j.conengprac.2023.105452
Received 15 June 2022; Received in revised form 26 January 2023; Accepted 26 January 2023
Available online 2 February 2023

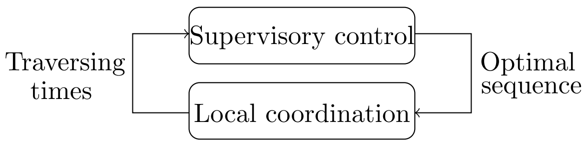

Fig. 1. Iterative learning and control. Supervisory control for the optimal sequencing and local motion coordination.

control problems (Ren, 2007). In Ren and Beard (2005) the authors develop a consensus algorithm to obtain coordination in multi-agent systems under dynamically changing communication topology.

This paper wishes to explore the ways in which existing sets of tools from the mentioned sectors can be adapted to the rail sector. To do this, the whole infrastructure necessitates of advanced information and communication capability on each vehicle. The ICT equipment in each rail vehicle allows the vehicle to create models of virtual couplings with the neighbor trains in the same spirit as in convoys of trains. This paper will distinguish between a supervisory control phase and a local coordination phase as depicted in Fig. 1. The supervisory control involves an optimization problem which builds on the notion of alternative graphs for conflict resolution in railways systems as developed in Corman et al. (2010), D'ariano et al. (2007), D'Ariano et al. (2007). While the models and methods for such an optimization problem are well established in the literature, this paper aims at reviewing them coupled with a local coordination algorithm. Indeed, in the spirit of learning, the arrows indicate that the parameters for the supervisory control can be obtained from the local coordination and vice versa. Thus the coupling between the two problems can be viewed as an iterative learning and control process. The output from the supervisory control is the optimal sequence which enters as input into the local coordination phase. The output from the local coordination phase yields the parameters values (traversing times) which enter as inputs in the supervisory control phase.

In the supervisory control phase, the control room makes economic decisions in the presence of conflict for a common resource. For instance, the supervisory control phase releases the optimal sequence with which the trains have to cross a junction. Such sequence is communicated to the trains through a ground antenna. The local coordination phase consists in each train to accelerate or decelerate to synchronize its relative position and velocity from the preceding train in the sequence and to guarantee the minimum safe headway. The computational burden for the local coordination is then shifted to the ICT equipment of each rail vehicle.

The main idea of this paper can be explained by the simple example illustrated in Fig. 2. Consider two tracks, one junction and three trains, which are labeled 1, 2 and 3, respectively. Trains 1 and 3 are on the same track while train 2 is on a second track and will join the main track through the junction. The trains communicate with a control room (supervisory control) via a central antenna (red dotted lines). At the same time the trains communicate with each other (blue dashed lines) relevant parameters such as position and velocity. Each train is equipped with internal computational power which identifies the virtual coupling configurations. The virtual coupling is assimilated to an array of masses connected in series via springs and dashpots. Before the junction, train 2 is on a different track than 1 and 3 and therefore in this phase train 2 is virtually projected on the main track. This is represented by a dashed rectangle representing mass 2 (array of masses bottom left). After projection and before the trains reach the junction, the trains receive the optimal sequence from the control room (supervisory control) which sees train 1 going first, train 3 following as second and eventually train 2 joining the convoy as last. Through distributed communication of the relative position and speed, the trains also realize that the virtual headway needs to increase. In consequence of this, the trains will control their velocity in order to move from the virtual coupling configuration before the junction (bottom left) to the virtual coupling configuration after the junction (bottom right). In particular, train 1 and 3 accelerate, while train 2 decelerates to reach the virtual coupling configuration represented on the bottom right. Local coordination between trains is then performed autonomously and with no supervision from the control room.

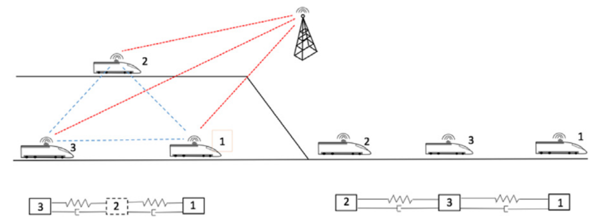

Fig. 2. Virtual coupling. Example of multiple trains virtually coupled.

1.1. Main theoretical findings

Cooperative control for rail vehicles is innovative in the following aspects.

Adaptation – Vehicles are autonomous entities equipped with ICT to share information with the control room and with the other trains. Each vehicle learns positions, and velocities and adapts its acceleration/deceleration command.

Coordination – Vehicles coordinate relative position and velocity to synchronize with the neighbor trains. First, a supervisory control received from the control room establishes the optimal sequence with which the trains cross junctions. Then, the trains implement a low-level coordination control to guarantee the necessary headway.

Prediction – Rail vehicles build forecasting models of virtual coupling based on the current information. Vehicles know in advance their relative position and velocity and anticipate any potential conflict or violation of safety conditions.

Structure – Rail vehicles communicate according to a communication topology, which can be described using a graph where the nodes represent the vehicles and the edges describe information sharing between vehicles.

The technical contribution of this paper is three-fold. First, for the single rail vehicle, a nonlinear Newtonian model is developed that accounts for nonlinearities due to uncertain aerodynamic forces and forces due to track slopes. Based on this model a constructive method is provided to design a feedback control that stabilizes the vehicle around a desired equilibrium point, in terms of position and velocity. The control design is in the spirit of reference model nonlinear control methods. Stability properties and oscillatory motions are analyzed in relation to certain bounds on the parameters' values (mass of the train, control parameters). These bounds shed light on the robustness properties of the control design. The stability properties are guaranteed for any value of the parameters within such bounds.

Second, the control design method is extended to the case of multiple virtually coupled vehicles. It is proven that the transient dynamics of the whole system follows a typical synchronization dynamics. It is also proven that under such control, the whole system of rail vehicles converges to a pre-defined equilibrium point, characterized by a specific velocity and relative distance between vehicles. Conditions for the stability of such equilibrium points are investigated.

Third, under the hypothesis of homogeneity, bounds on the damping coefficient for the synchronization equilibrium are provided (in terms of velocity and relative distance between vehicles) to be overdamped or underdamped. The importance of such result is in that it sheds light on the emergence of topology-induced oscillations. These bounds depend on the interaction topology and on the connectivity of the vehicles. The maximum connectivity corresponds to the maximum number of links over all the nodes of an ad hoc network, where nodes are vehicles and links are communication channels.

This paper is organized as follows. In Section 2, models and methods for the supervisory control are reviewed. In Section 3, the model and control of a single vehicle are developed. In Section 4, the model is extended to multiple rail vehicles. In Section 5, the control method is illustrated for the virtually coupled vehicles. In Section 6, the simulations are carried out. Finally, in Section 7, the conclusions and future works are discussed.

2. Supervisory control

Models and methods for the supervisory control are well established in the literature (Corman et al., 2010; D'ariano et al., 2007; D'Ariano et al., 2007). In this section, a review with an example is provided and the connection with the local coordination phase is clarified. The supervisory control finds the optimal sequence with which the trains have to cross a junction. The optimization problem builds on the notion of alternative graphs. An alternative graph is a triple $G(N, F, A)$ where N is the set of nodes, F is the set of fixed arcs and A is the set of alternative arcs. Let $|N|$ be the cardinality of set N. A subset $S \subset A$ involving one arc for each pair in A has to be chosen to obtain the final graph $G(S) = (N, F \cup S)$. To obtain the model, for each pair of arcs (i, j), (h, k) in A consider the variable

$$y_{ij,hk} = \begin{cases} 1, & \text{if } (i,j) \text{ selected}, \\ 0, & \text{if } (h,k) \text{ selected}. \end{cases}$$

Also, let $\tau_i \in \mathbb{R}$ be the decision variable associated with node i which represents the starting time of event i. Denote by ϕ_{ij} the weight of arc (i, j) which describes the duration of event i for each fixed arc $(i, j) \in F$. Likewise, denote by β_{ij} and β_{hk} the weights of arcs (i, j) and (h, k) which describe the duration of events i and h for each alternative arc $(i, j), (h, k) \in A$. Let $\hat{M}$ be a sufficiently large number. Denote by $\Phi(\tau_1, \dots, \tau_{|N|})$ a generic (non)linear function of the decision variables, then a mixed-integer (non)linear program can be obtained as follows,

$$\begin{aligned} & \min \Phi(\tau_1, \dots, \tau_{|N|}) \\ & \tau_j \geq \tau_i + \phi_{ij}, && \forall (i,j) \in F, \\ & \begin{cases} \tau_j \geq \tau_i + \beta_{ij} - \hat{M}(1 - y_{ij,hk}), \\ \tau_k \geq \tau_h + \beta_{hk} - \hat{M} y_{ij,hk}, \\ y_{ij,hk} \in \{0, 1\}. \end{cases} && \forall (i,j), (h,k) \in A, \end{aligned}$$

If the events are viewed as times when trains occupy or free a block section, then selecting alternative arcs corresponds to sequencing the trains as explained in the following example.

Example 1. Two trains need to occupy Block section 3, see Fig. 3 left. Train 1 comes from Block section 1 (BS 1) and Train 2 from Block section 2 (BS 2). The trains cannot occupy Block section 3 (BS 3) at the same time. Let r_1 and r_2 be the traversing time of Block sections 1 and 2, respectively (this is the time before the trains are ready to enter Block section 3). Let ϕ_{12} and ϕ_{34} be the traversing time of Block section 3 for Train 1 and 2, respectively. If Train 1 enters Block section 3 first, let β_{23} be the idle interval between the time when Train 1 leaves Block section 3 and Train 2 enters Block section 3. Analogously, if Train 2 enters Block section 3 first, let β_{41} be the idle interval between the time when Train 2 leaves Block section 3 and Train 1 enters Block section 3.

The alternative graph in Fig. 3 (right) can be used to visualize the different stages of the scheduling process. The nodes are the "events" (Train 1 or 2 entering or exiting Block section 3) and the arcs are the jobs (Train 1 and 2 traversing Block section 3 or idle time before the next train can enter Block section 3). In particular, let τ_1 and τ_2 be the time of Train 1 entering and exiting Block section 3, respectively.

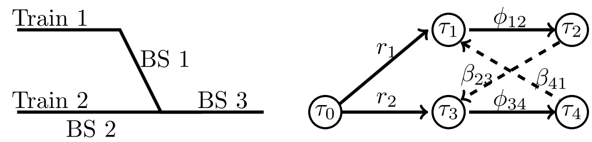

Fig. 3. Supervisory control. Example with two trains and three block sections (BS) (left); corresponding alternative graph (right).

Analogously, let τ_3 and τ_4 be the time of Train 2 entering and exiting Block section 3. For this particular instance, the decision variable is

$$y_{23,41} = \begin{cases} 1 & \text{if Train 1 precedes 2 in Block section 3}, \\ 0 & \text{otherwise}. \end{cases}$$

The mixed-integer program to minimize the total completion time (Case 1) or the average completion time (Case 2) is then given by

$$\text{Case 1:} \quad \min \max\{\tau_2, \tau_4\} \; \left(\text{Case 2:} \quad \min \tau_2 + \tau_4\right) \tag{1}$$

$$\tau_2 \geq \tau_1 + \phi_{12}, \tag{2}$$

$$\tau_4 \geq \tau_3 + \phi_{34}, \tag{3}$$

$$\tau_3 \geq \tau_2 + \beta_{23} - \hat{M}(1 - y_{23,41}), \tag{4}$$

$$\tau_1 \geq \tau_4 + \beta_{41} - \hat{M} y_{23,41}, \tag{5}$$

$$\tau_1 \geq r_1, \tag{6}$$

$$\tau_3 \geq r_2, \tag{7}$$

$$y_{23,41} \in \{0, 1\}. \tag{8}$$

The objective function (1) describes the total completion time (Case 1) or average completion time (Case 2). Constraint (2) says that Train 1 cannot exit Block section 3 before it has entered at time τ_1 and it has occupied Block section 3 for ϕ_{12} time units. Constraint (3) imposes that Train 2 cannot exit Block section 3 before it has entered at time τ_3 and it has occupied Block section 3 for ϕ_{34} time units. Constraint (4) describes the condition that if Train 1 precedes 2, Train 2 cannot enter Block section 3 (at time τ_3) before Train 1 has exited (at time τ_2) and the idle time interval β_{23} has passed. Constraint (5) captures the condition that if Train 2 precedes 1, Train 1 cannot enter Block section 3 (at time τ_1) before Train 2 has exited (at time τ_4) and the idle time interval β_{41} has passed. Finally, condition (6) says that Train 1 cannot enter Block section 3 (at time τ_1) before traversing Block section 1 for a time r_1. Likewise (7) says that Train 2 cannot enter Block section 3 (at time τ_3) before traversing Block section 2 for a time r_2. In (8) the variable is integer, as it corresponds to mutually exclusive decisions.

3. Nonlinear model of a single rail vehicle

Consider a single rail vehicle and let $v(t)$ and $p(t)$ be its velocity and position at time t, respectively. The model builds on the longitudinal train dynamics proposed in Felez et al. (2019), Iwnicki (2006), Wu et al. (2016). Let F be the engine thrust, $f_1(v, t)$ be the aerodynamic forces (essentially drag resistance to motion) and $f_2(p, v, t)$ be any external force due to track slope and geometry.

For a vehicle of mass M the velocity $v(t)$ evolves as

$$M\dot{v}(t) = F - f_1(v, t) - f_2(p, v, t), \tag{9}$$

where $f_1(v, t) = a + bv(t) + cv^2(t)$ is taken in accordance with Davis approximation (Dong et al., 2016). Here the coefficient a involves the rolling resistance and the bearing resistance; the coefficient b captures the air input and c includes the aerodynamic coefficient and the tunnel factor. Estimating the aforementioned coefficients is not required as the model and method presented in this paper can accommodate unknown parameters values but bounded within certain intervals. More details on the coefficients' estimation can be found in Hansen et al. (2017). Let the engine thrust be decomposed in two components, namely

$F(t) = F_1(t) + F_2(t)$. The first component $F_1(t)$ has to be designed to counterbalance $f_1(v,t)$ and $f_2(p,v,t)$. For the second component, let $p_d(t)$ and $v_d(t)$ be two virtual signals representing the desired position and velocity, respectively. The second component $F_2(t)$ is designed to guarantee tracking, namely $F_2(t) = ke(t) + \tilde{k}\dot{e}(t)$, where $e(t) = p_d(t) - p(t)$ and $\dot{e}(t) = \dot{p}_d(t) - \dot{p}(t) = v_d(t) - v(t)$ are the position and velocity tracking error and k and $\tilde{k}$ are positive scalars representing the synchronization coefficients. Dynamics (9) can then be rewritten as

$$M\dot{v} \quad = F_1 + ke + \tilde{k}\dot{e} - f_1(v,t) - f_2(p,v,t). \tag{10}$$

The synchronization coefficients determine the engine thrust $F_2(t) = ke(t) + \tilde{k}\dot{e}(t)$. In other words, the acceleration $\dot{v}(t)$ depends on the engine thrust $F_2(t) = ke(t) + \tilde{k}\dot{e}(t)$, on the drag resistance to motion $f_1(v,t) = a + bv(t) + cv^2(t)$ and on the external disturbances due to the track $f_2(p,v,t)$. The physical intuition underlying the design of $F_2(t)$ is that in response to a positive error, an engine thrust power is injected into the rail vehicle. Vice versa, a negative error induces the engine thrust power to decrease. Denoting $p(t) = x_1(t)$, $v(t) = x_2(t)$, and by considering $p_d(t) = x_1^d(t)$ and $v_d(t) = x_2^d(t)$ as exogenous inputs to the rail vehicle, the dynamics of the rail vehicle reduces to the following second-order system:

$$\begin{aligned} \begin{bmatrix} \dot{x}_1 \\ \dot{x}_2 \end{bmatrix} &= \begin{bmatrix} 0 & 1 \\ -\frac{k}{M} & -\frac{\tilde{k}}{M} \end{bmatrix} \begin{bmatrix} x_1 \\ x_2 \end{bmatrix} \\ &+ \begin{bmatrix} 0 & 0 \\ \frac{k}{M} & \frac{\tilde{k}}{M} \end{bmatrix} \begin{bmatrix} x_1^d \\ x_2^d \end{bmatrix} - \begin{bmatrix} 0 \\ \frac{a+bx_2+cx_2^2+f_2-F_1}{M} \end{bmatrix}. \end{aligned} \tag{11}$$

Assume parameters are unknown but bounded, namely $a \in [-\underline{a}, \overline{a}]$, $b \in [-\underline{b}, \overline{b}]$, and $c \in [-\underline{c}, \overline{c}]$ and $f_2 \in [\underline{f}_2, \overline{f}_2]$ in which case F_1 can be designed via feedback from the error. The error is obtained via model reference control as discussed next.

Consider the following *reference model* for the vehicle:

$$\begin{bmatrix} \dot{\hat{x}}_1 \\ \dot{\hat{x}}_2 \end{bmatrix} = \begin{bmatrix} 0 & 1 \\ -\frac{k}{M} & -\frac{\tilde{k}}{M} \end{bmatrix} \begin{bmatrix} \hat{x}_1 \\ \hat{x}_2 \end{bmatrix} + \begin{bmatrix} 0 & 0 \\ \frac{k}{M} & \frac{\tilde{k}}{M} \end{bmatrix} \begin{bmatrix} x_1^d \\ x_2^d \end{bmatrix}. \tag{12}$$

Consider the error on position and velocity $\hat{e}_1 = x_1^d - \hat{x}_1$ and $\hat{e}_2 = x_2^d - \hat{x}_2$ and let the error dynamics be derived under the assumption of quasi-constant desired velocity, namely $\dot{x}_2^d \approx 0$:

$$\begin{bmatrix} \dot{\hat{e}}_1 \\ \dot{\hat{e}}_2 \end{bmatrix} = \begin{bmatrix} 0 & 1 \\ -\frac{k}{M} & -\frac{\tilde{k}}{M} \end{bmatrix} \begin{bmatrix} \hat{e}_1 \\ \hat{e}_2 \end{bmatrix}. \tag{13}$$

The equilibrium point for the reference model is then

$$\lim_{t\to\infty} \hat{x}_1 = x_1^d, \quad \lim_{t\to\infty} \hat{x}_2 = x_2^d.$$

Let the error on position and velocity be defined as $\epsilon_1 = \hat{x}_1 - x_1$ and $\epsilon_2 = \hat{x}_2 - x_2$.

Theorem 1. *Let F_1 be designed as a feedback control from the tracking error for positive parameters μ and $\tilde{\mu}$:*

$$F_1 = \mu\epsilon_1 + \tilde{\mu}\epsilon_2. \tag{14}$$

At the equilibrium

$$\begin{bmatrix} x_1 \\ x_2 \end{bmatrix} = \begin{bmatrix} x_1^d - \frac{a+bx_2(t)+cx_2^2(t)+f_2(x_1,x_2,t)}{k+\mu} \\ x_2^d \end{bmatrix}. \tag{15}$$

The transient dynamics of the reference model coincides with the rail vehicle's dynamics under perfect information. Perfect information means that the aerodynamic forces $f_1(v,t)$ and any external force due to track slope and geometry, $f_2(p,v,t)$ are known or can be calculated online. Through feedback linearization, let F_1 be chosen as $F_1 = a + bv(t) + cv^2(t)$. The linear approximation leads to

$$M\dot{v}(t) \approx -ke(t) - \tilde{k}\dot{e}(t). \tag{16}$$

The dynamics for $v(t)$ follows then

$$\dot{v}(t) \approx \frac{1}{M}\left(-ke(t) - \tilde{k}\dot{e}(t)\right), \tag{17}$$

where $\frac{k}{M}$ and $\frac{\tilde{k}}{M}$ are the elastic and damping constant of the linearized dynamics, respectively. Dynamics (17) can be written in matrix form as follows:

$$\begin{bmatrix} \dot{x}_1 \\ \dot{x}_2 \end{bmatrix} = \underbrace{\begin{bmatrix} 0 & 1 \\ -\frac{k}{M} & -\frac{\tilde{k}}{M} \end{bmatrix}}_{A} \begin{bmatrix} x_1 \\ x_2 \end{bmatrix} + \begin{bmatrix} 0 & 0 \\ \frac{k}{M} & \frac{\tilde{k}}{M} \end{bmatrix} \begin{bmatrix} x_1^d \\ x_2^d \end{bmatrix}. \tag{18}$$

Theorem 2. *Dynamics (18) is asymptotically stable. Furthermore, let $\tilde{k} > 2\sqrt{kM}$ then the origin is an asymptotically stable node. Vice versa, if $\tilde{k} < 2\sqrt{kM}$ then the origin is an asymptotically stable spiral.*

The above theorem explains the impact of the mass and the elastic/damping constant on the vehicle's dynamics. Furthermore, it makes the results of this paper robust and extends the analysis to cases where the inertia, damping and synchronization parameters are uncertain.

4. Virtual coupling

Virtual coupling consists in creating a virtual network $G = (V, E)$ of interconnected vehicles, where the set V is the set of nodes which correspond to vehicles, and the set E is the set of arcs, which correspond to virtual couplings between vehicles. Two vehicles are called neighbors if there exists a link between the two corresponding nodes. Thus, a measure of the connectivity of a vehicle is the degree of the corresponding node. Recall that for undirected graphs, the degree of a node is the number of links with end node i; here, the degree of node i is denoted by d_i.

For any pair of vehicles i and j, let the velocity tracking error and synchronization coefficient be k_{ij} and $\tilde{k}_{ij}$, respectively. The new aggregate parameters are defined as $k_{ij} := k\mu_{ij}$, and $\tilde{k}_{ij} := \tilde{k}\tilde{\mu}_{ij}$, where $\sum_j \mu_{ij} = \sum_j \tilde{\mu}_{ij} = 1$, and $k, \tilde{k}$ are positive scalars to be designed yet. Note that it holds $\sum_j k_{ij} = k$ and $\sum_j \tilde{k}_{ij} = \tilde{k}$. Also, let ξ be the synchronization coefficient with respect to a reference velocity v_{ref}.

For a generic vehicle i let the new state space variable be $x_1^i(t) = p_i(t) - \delta_i$, where $p_i(t)$ is the position of vehicle i and δ_i is a positive scalar which can be designed ad hoc and will determine the relative distance between vehicle i and the neighbor vehicles. Also let $x_2^i(t) = v_i(t)$.

Lemma 1. *The single vehicle i admits the following state space representation*

$$\begin{aligned} &M\dot{x}_2^i(t) = \textstyle\sum_j k_{ij}(x_1^j(t) - x_1^i(t)) + \sum_j \tilde{k}_{ij}(x_2^j(t) - x_2^i(t)) \\ &+\xi(v_{ref}(t) - x_2^i(t)) - f_1(v_i,t) - f_2(p_i,v_i,t) + F_1^i. \end{aligned} \tag{19}$$

To describe the whole set of coupled vehicles in one single matrix model, let the aerodynamic and external forces of vehicle i be denoted as $f_1^i = f_1(v_i,t)$ and $f_2^i = f_2(p_i,v_i,t)$, respectively, and let $f_{12}^i := f_1^i + f_2^i$. Also, let the velocity error of vehicle i with respect to a reference value be denoted by $e_v^i := v_{ref} - x_2^i$. The dynamics of the whole set of virtually coupled vehicles are then given by:

$$\begin{bmatrix} \dot{X}_1 \\ \dot{X}_2 \end{bmatrix} = \begin{bmatrix} 0 & 1 \\ -L & -\tilde{L} \end{bmatrix} \begin{bmatrix} X_1 \\ X_2 \end{bmatrix} + \Psi(X_2) - \Delta(X_1,X_2) + \tilde{F}, \tag{20}$$

where $X_i = [x_i^1, \dots, x_i^n]^T$, $i = 1, 2$,

$$\Psi(X_2) := \begin{bmatrix} 0 & \dots & 0 & \frac{\xi e_v^1}{M_1} & \dots & \frac{\xi e_v^n}{M_n} \end{bmatrix}^T,$$

$$\Delta(X_1,X_2) := \begin{bmatrix} 0 & \dots & 0 & \frac{f_1(x_2^1,t)+f_2(x_1^1,x_2^1,t)}{M_1} & \dots & \frac{f_1(x_2^n,t)+f_2(x_1^n,x_2^n,t)}{M_n} \end{bmatrix}^T,$$

$$\tilde{F} := \begin{bmatrix} 0 & \dots & 0 & \frac{F_1^1}{M_1} & \dots & \frac{F_1^n}{M_n} \end{bmatrix}^T.$$

In the equations above $\Delta(X_1,X_2)$ denotes the disturbance affecting the dynamics of the whole set of virtually coupled vehicles. In these equations, the block matrices $L = [l_{ij}]_{i,j\in\{1,\dots,n\}}$ and $\tilde{L} = [\tilde{l}_{ij}]_{i,j\in\{1,\dots,n\}}$ are used which represent the Laplacian matrices of the interconnected graph. For a generic weighted graph, the corresponding entries of L are given by

$$l_{ij} = \begin{cases} -\frac{k_{ij}}{M_i} & \text{if } i \neq j, \\ \frac{1}{M_i} \sum_{h=1,h\neq i} k_{ih} & \text{if } i = j, \end{cases} \tag{21}$$

and similarly for $\tilde{L}$ by replacing k_{ij} with $\tilde{k}_{ij}$. Note that the row-sums of a Laplacian matrix are zero. Furthermore, the matrix has nonnegative diagonal entries and nonpositive non-diagonal entries.

5. Virtual couplings and reference model

Consider the following reference model which is obtained by ignoring the forces f_1^i and f_2^i.

$$\begin{bmatrix} \dot{\hat{x}}_1 \\ \dot{\hat{x}}_2 \end{bmatrix} = \begin{bmatrix} 0 & 1 \\ -L & -\tilde{L} \end{bmatrix} \begin{bmatrix} \hat{x}_1 \\ \hat{x}_2 \end{bmatrix} + \begin{bmatrix} 0 \\ \hat{e}_v \end{bmatrix},$$

where $\hat{e}_v = [\frac{\xi(v_{ref}(t)-\hat{x}_2^1(t))}{M_1} \dots \frac{\xi(v_{ref}(t)-\hat{x}_2^n(t))}{M_n}]^T$. The author in Ren (2007) showed that for the above system it holds $\lim_{t\to\infty} \hat{x}_1^i(t) = x_{ref}$ and $\lim_{t\to\infty} \hat{x}_2^i(t) = v_{ref}$ for all $i \in V$, where $x_{ref}(t) = \int_0^t v_{ref}(\tau)d\tau + x_{ref}(0)$ for given $x_{ref}(0)$ and $v_{ref}(\tau)$ in [0,t). To see this, consider the following dynamics

$$\begin{bmatrix} \mathbf{1}\dot{x}_{ref} \\ \mathbf{1}\dot{v}_{ref} \end{bmatrix} = \begin{bmatrix} 0 & 1 \\ -L & -\tilde{L} \end{bmatrix} \begin{bmatrix} \mathbf{1}x_{ref} \\ \mathbf{1}v_{ref} \end{bmatrix}.$$

Define $\hat{x}_j := [\hat{x}_j^i]_{i\in V}$ for $j = 1,2$ and introduce $\bar{e}_1 = \hat{x}_1 - \mathbf{1}x_{ref}$ and $\bar{e}_2 = \hat{x}_2 - \mathbf{1}v_{ref}$. Then

$$\begin{bmatrix} \dot{\bar{e}}_1 \\ \dot{\bar{e}}_2 \end{bmatrix} = \begin{bmatrix} 0 & 1 \\ -L & -\tilde{L} - diag(\frac{\xi}{M_i}) \end{bmatrix} \begin{bmatrix} \bar{e}_1 \\ \bar{e}_2 \end{bmatrix}.$$

In the case of a homogeneous network, take for instance $M_i \approx 1$ for all $i \in V$, the above system can be written as

$$\lim_{t\to\infty} \bar{e}_1(t) = \mathbf{1}p^T \bar{e}_1(0) + \frac{1}{\xi}\mathbf{1}p^T \bar{e}_2(0), \quad \lim_{t\to\infty} \bar{e}_2(t) = \mathbf{0}, \tag{22}$$

where p is the left eigenvector of L and $p^T\mathbf{1} = 1$. Then it can concluded that for all $i \in V$

$$\begin{bmatrix} \hat{x}_1^i(t) \\ \hat{x}_2^i(t) \end{bmatrix} \to \begin{bmatrix} p^T \bar{e}_1(0) + \frac{1}{\xi} p^T \bar{e}_2(0) + \int_0^t v_{ref}(\tau)d\tau \\ v_{ref} \end{bmatrix}. \tag{23}$$

Based on the above reference model, the error which measures the deviation of the actual position and velocity from the reference ones can be defined as:

$$\begin{bmatrix} e_1^i \\ e_2^i \end{bmatrix} = \begin{bmatrix} \hat{x}_1^i - x_1^i \\ \hat{x}_2^i - x_2^i \end{bmatrix}. \tag{24}$$

Define the following matrix

$$\mathcal{A} := \begin{bmatrix} 0 & 1 \\ -L - diag(\frac{\mu}{M_i}) & -\tilde{L} - diag(\frac{\xi+\tilde{\mu}}{M_i}) \end{bmatrix}.$$

Theorem 3. *Design F_1 as a feedback control from the tracking error for positive parameters μ and $\tilde{\mu}$*

$$F_1 = \mu e_1^i + \tilde{\mu} e_2^i. \tag{25}$$

At the equilibrium the following equation holds

$$\begin{bmatrix} X_1^* \\ X_2^* \end{bmatrix} = \begin{bmatrix} \hat{X}_1^* \\ \hat{X}_2^* \end{bmatrix} + \mathcal{A}^{-1}\Delta(X_1^*, X_2^*), \tag{26}$$

where

$$\begin{bmatrix} \hat{X}_1^* \\ \hat{X}_2^* \end{bmatrix} = \begin{bmatrix} \mathbf{1}(p^T \bar{e}_1(0) + \frac{1}{\xi} p^T \bar{e}_2(0) + \int_0^t v_{ref}(\tau)d\tau) \\ \mathbf{1}v_{ref} \end{bmatrix}.$$

Theorem 4. *Let a network of interconnected homogeneous rail vehicles be given, and the equilibrium point (26). The equilibrium point (26) is asymptotically stable, i.e.*

$$\lim_{t\to\infty} X_i(t) = X_i^*, \quad i = 1,2.$$

Furthermore, let $\frac{\xi+\tilde{\mu}}{M} - \eta_i > \sqrt{4\frac{\mu}{M} - \eta_i}$ for all $i = 1,\dots,n$, then the equilibrium point (26) is an asymptotically stable node, where η_i is the ith eigenvalue of $-L$. Vice versa, if $\frac{\xi+\tilde{\mu}}{M} - \eta_i < \sqrt{4\frac{\mu}{M} - \eta_i}$ for some $i = 1,\dots,n$, then the equilibrium point (26) is an asymptotically stable spiral.

The next result provides conditions on the parameters that guarantee no oscillation in the virtually coupled dynamics of the interconnected vehicles.

Corollary 1. *All eigenvalues λ_i^+, λ_i^- for $i = 1,\dots,n$ are real and negative if $-M + \xi + \tilde{\mu} > \mu$.*

Example 2 (*Two virtually coupled vehicles*). In the case of two vehicles that are virtually coupled the dynamics can be rewritten as

$$\begin{bmatrix} \dot{e}_1^1 \\ \dot{e}_1^2 \\ \dot{e}_2^1 \\ \dot{e}_2^2 \end{bmatrix} = \begin{bmatrix} 0 & 0 & 1 & 0 \\ 0 & 0 & 0 & 1 \\ l_{11}^{\mu} & l_{12} & \tilde{l}_{11}^{\xi\tilde{\mu}} & \tilde{l}_{12} \\ l_{21} & l_{22}^{\mu} & \tilde{l}_{21} & -\tilde{l}_{22}^{\xi\tilde{\mu}} \end{bmatrix} \begin{bmatrix} e_1^1 \\ e_1^2 \\ e_2^1 \\ e_2^2 \end{bmatrix} + \begin{bmatrix} 0 \\ 0 \\ \frac{f_{12}^1}{M_1} \\ \frac{f_{12}^2}{M_2} \end{bmatrix} \tag{27}$$

where

$$l_{ii}^{\mu} := -l_{ii} - \frac{\mu}{M_i}, \quad \tilde{l}_{ii}^{\xi\tilde{\mu}} := -\tilde{l}_{ii} - \frac{\xi+\tilde{\mu}}{M_i}.$$

For a given scalar $\kappa > 0$, the Laplacian of the weighted graph is given by

$$\tilde{L} = L = \begin{bmatrix} \frac{\kappa}{M_1} & 0 \\ 0 & \frac{\kappa}{M_2} \end{bmatrix} \begin{bmatrix} 1 & -1 \\ -1 & 1 \end{bmatrix}. \tag{28}$$

To obtain the eigenvalues of the above matrix, calculate $Tr(A) = \frac{\kappa}{M_1} + \frac{\kappa}{M_2}$, where $Tr(A)$ is the trace of matrix A and from $\Delta(A) = \frac{\kappa^2}{M_1M_2} - \frac{\kappa^2}{M_1M_2} = 0$, where $\Delta(A)$ is the determinant of matrix A. Recall that stability depends on the eigenvalues of A and that the expression of the eigenvalues is given by

$$\eta_{1,2} = \frac{Tr(A)\pm\sqrt{Tr(A)^2-4\Delta(A)}}{2} \in \{0, \frac{\kappa}{M_1} + \frac{\kappa}{M_2}\}. \tag{29}$$

Then from Theorem 4, if $M_1 \approx M_2$ it can be inferred that

- All eigenvalues λ_i^+, λ_i^- for $i = 1,2$ are real and negative if $\frac{\xi+\tilde{\mu}}{M} - \eta_i > \sqrt{4\frac{\mu}{M} - \eta_i}$ for $\eta_i \in \{0, 2\frac{\kappa}{M}\}$.
- There exists one complex eigenvalue/eigenmode if $\frac{\xi+\tilde{\mu}}{M} - \eta_i < \sqrt{4\frac{\mu}{M} - \eta_i}$ for at least one value of $\eta_i \in \{0, 2\frac{\kappa}{M}\}$.

6. Simulations

The simulations are conducted to corroborate the effectiveness of the proposed control method. The simulations are conducted in a Matlab environment. All tests are performed on PC Intel Core i7 − 1185G7 (3 GHz) with 16 GB RAM. The simulated scenario involves two tracks, one junction and five rail vehicles as illustrated in Fig. 4. Track 2 connects to track 1 through a junction. The initial configuration before the junction is red–blue–cyan–green–black (2 − 1 − 3 − 5 − 4). The desired final configuration after the junction is blue–red–cyan–black–green (1 − 2 − 3 − 4 − 5). The communication topology is a chain as illustrated in Fig. 5. The sequence of nodes in the chain is the same as in the final configuration.

The numerical studies involve three sets of simulations. The dynamics in (20) are simulated where $\Delta(X_1(t), X_2(t))$ is generated randomly in a predefined interval as clarified later, and F_1 is calculated in

Table 1
Position tracking error results. Position tracking error $e(t)$ in the case of (a) disturbance but no feedback control $\tilde{F}$, (b) disturbance and feedback control $\tilde{F}$ as in (20), where F_1 is defined in (25). All the entries of the table are m.

	t = 10 s		t = 30 s		t = 50 s		t = 70 s		t = 90 s	
Train	Case (a)	Case (b)	Case (a)	Case (b)	Case (a)	Case (b)	Case (a)	Case (b)	Case (a)	Case (b)
1	71.05	29.20	315.90	63.27	569.05	80.50	822.17	93.46	1082.1	101.45
2	84.39	27.03	321.00	72.99	565.18	85.64	823.39	93.13	1075.8	97.01
3	81.30	17.51	327.80	64.69	579.50	88.40	836.99	85.85	1088.3	88.71
4	80.59	30.29	328.37	59.15	579.34	81.83	846.40	89.86	1099.3	87.34
5	74.62	31.35	312.97	63.21	572.70	92.03	840.47	102.84	1097.4	85.71

Table 2
Speed tracking error results. Speed tracking error $\dot{e}(t)$ in the case of (a) disturbance but no feedback control $\tilde{F}$, (b) disturbance and feedback control $\tilde{F}$ as in (20), where F_1 is defined in (25). All the entries of the table are km/h.

	t = 10 s		t = 30 s		t = 50 s		t = 70 s		t = 90 s	
Train	Case (a)	Case (b)	Case (a)	Case (b)	Case (a)	Case (b)	Case (a)	Case (b)	Case (a)	Case (b)
1	10.37	2.04	14.51	2.49	13.11	0.80	16.04	0.41	15.40	0.88
2	14.48	0.80	10.08	2.05	11.09	0.75	15.66	0.29	10.23	2.30
3	13.17	2.24	12.87	0.90	12.12	1.78	11.77	1.29	11.20	1.91
4	12.09	0.36	14.52	0.12	11.93	1.98	10.99	0.34	12.59	0.13
5	11.70	4.78	15.56	3.09	15.92	2.36	11.47	0.74	12.25	0.96

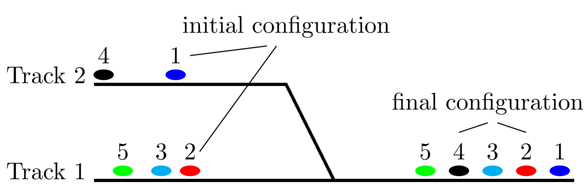

Fig. 4. Simulation example. Two tracks, one junction and five trains, initial configuration before the junction (left) and final configuration after the junction (right).

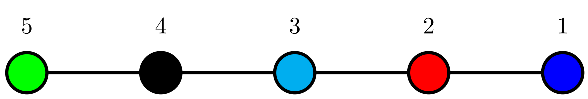

Fig. 5. Chain communication topology. Each train communicates with the preceding and following ones.

accordance to (25). The parameters values are set as follows: step size $dt = 0.05$; horizon window $T = 100$ iterations; reference velocity $v_{ref} = 40$ km/h (approximately 11 m/s) before the junction and $v_{ref} = 70$ km/h (approximately 19.5 m/s) after the junction; synchronization parameters $-\frac{k_{ij}}{M_i} = 6$ and $-\frac{\tilde{k}_{ij}}{M_i} = 1.8$ respectively for every pair of connected trains $i \neq j$ otherwise both parameters are zero; the mass of vehicle i is $M_i \approx 1$; the positive parameters in the feedback controller are $\mu = \tilde{\mu} = 10$; the synchronization parameter with respect to the reference velocity is $\xi = 4$; the disturbance Δ is in the interval $[-100, 0]$; the offset of the vehicles are $\delta_1 = 0$, $\delta_2 = 25$, $\delta_3 = 50$, $\delta_4 = 75$, $\delta_5 = 100$, $\delta_6 = 125$.

Time is measured in "second", and the horizon is 100 s time units. Distance is measured in "meter" and takes values in the interval from 0 to 2000 m. Figs. 6(a)–(f) depict samples of the dynamics in terms of the geographic position of the vehicles (top) and distance and speed (middle and bottom). In particular, the dynamics is sampled at $t = 10$ s, 20 s, 30 s, 50 s, 70 s, 90 s. Between $t = 10$ s and $t = 30$ s the first train in track 2 overtakes the first train in track 1. Between $t = 10$ s and $t = 50$ s, the last train in track 2 overtakes the last train in track 1. The last train joining the convoy decreases its speed from above 60 km/h to below 20 km/h before $t = 20$ s to reach a safe distance from the preceding trains and then slowly accelerates to converge to the reference velocity $v_{ref} = 40$ km/h before passing the junction. At about $t = 50$ s, the last train in the convoy reaches the junction and the reference speed changes from 40 km/h to 70 km/h. During the first 50 s, the speed dynamics follows a typical consensus dynamics where the consensus value is the reference speed $v_{ref} = 40$ km/h. Thus synchronization has already occurred at $t = 50$ s. During the second 50 s, the trains remain synchronized but increase the speed to reach the new reference value $v_{ref} = 70$ km/h, see the bottom plots. The distance between trains is constant, see the middle plots.

Fig. 7 depicts the distance and speed of the train vehicles, respectively, in the cases where a) there is no disturbance affecting the dynamics, namely $\Delta(X_1, X_2) = 0$ at any time, b) there is a disturbance, namely $\Delta(X_1, X_2) \neq 0$ but the feedback control $\tilde{F}$ is not implemented, c) there is a disturbance and the feedback control $\tilde{F}$ as in (20), where F_1 is defined in (25), tracks the position and speed at the reference values while guaranteeing the safety relative distance between the vehicles. Note that in Fig. 7(b), the disturbance slows down all the vehicles and impacts the synchronization process. Therefore, the converging value for the position is different from the desired one. Analogously note that the distance covered by the whole convoy is shorter if compared with the distance covered in (a) (no disturbance) and (c) (controlled dynamics). The colors of the plots match the color associated with each train. The gray shadowed region around each plot identifies the safety distance between two consecutive trains. A change of the slope of the plots can be observed in correspondence to a change of the reference velocity. While in (a) and (c) this occurs after all the trains have passed the junction, in (b) this occurs while some trains are still before the junction.

As it can be seen in Fig. 7, the plots follow a consensus dynamics where the speeds of trains first converge to 40 km/h during the first half of the horizon (while the $v_{ref} = 40$ km/h) and then converge to 70 km/h in the second half of the horizon (while the $v_{ref} = 70$ km/h). The influence of the disturbance is evident in Fig. 7(b), where the different speeds hardly synchronize around the reference speed.

Tables 1 and 2 illustrate the position and the speed tracking errors in the cases of disturbance but no feedback control $\tilde{F}$, disturbance and feedback control $\tilde{F}$ as in (20), where F_1 is defined in (25). The position tracking error $e(t)$ and the speed tracking $\dot{e}(t)$ are defined in Section 3. According to Table 1, the trains cover shorter distances in the first case compared to the second one. In the case of controlled dynamics, the whole convoy converges to the reference speed resulting in less position tracking error after the junction. As can be seen in Table 2, the speeds of trains in the presence of disturbance but no feedback control are at least 10 km/h units less than the desired speed. On the other hand, the speed tracking errors are smaller in the case of the controlled dynamics because trains synchronize their speeds

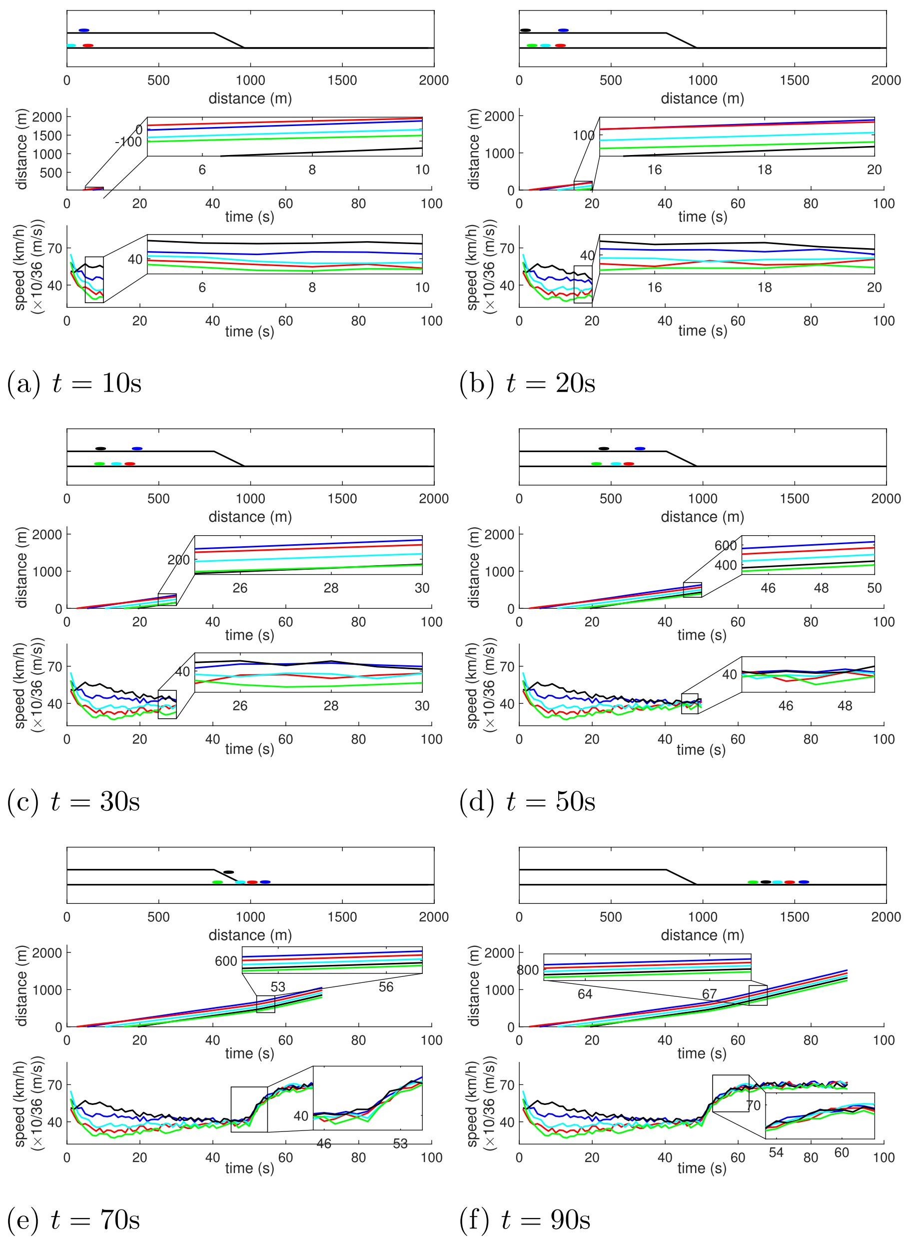

(a) $t = 10$s (b) $t = 20$s (c) $t = 30$s (d) $t = 50$s (e) $t = 70$s (f) $t = 90$s

Fig. 6. First set of simulations. Geographic position of the vehicles (top) and plot of distance (middle) and speed (bottom) at different times $t = 10$ s, 20 s, 30 s, 50 s, 70 s, 90 s.

around the reference speed before and after the junction. It is worth emphasizing that feedback control improves the convoy's performance in the presence of disturbances.

7. Conclusions

This paper develops models and studies transient dynamics for a single rail vehicle and multiple virtually coupled rail vehicles. In the spirit of cooperative control, a control design method is provided to guarantee synchronization as well as transient performances of the whole system. Results show robust properties of the control method when the parameters are bounded within intervals. Future works involve the extension of the results to the case where the parameters of the vehicles and of the feedback control change with time or are uncertain.

Declaration of competing interest

The authors declare that they have no known competing financial interests or personal relationships that could have appeared to influence the work reported in this paper.

Acknowledgments

This paper was supported by the SMiLES Research Project, part of the Research Programme Sustainable Living Labs, which is co-financed by the Dutch Research Council (NWO), the Ministry of Infrastructure and Water Management, The Netherlands, the Taskforce for Applied Research (SIA), The Netherlands and the Top Sector Logistics, The Netherlands. The first author would like to thank M. Glover, D. Gill, A. Powell, and A. Woods at *Siemens Automation* and Nadia Hoodbhoy at *Network Rail* for sharing fruitful thoughts during the early stages of this work.

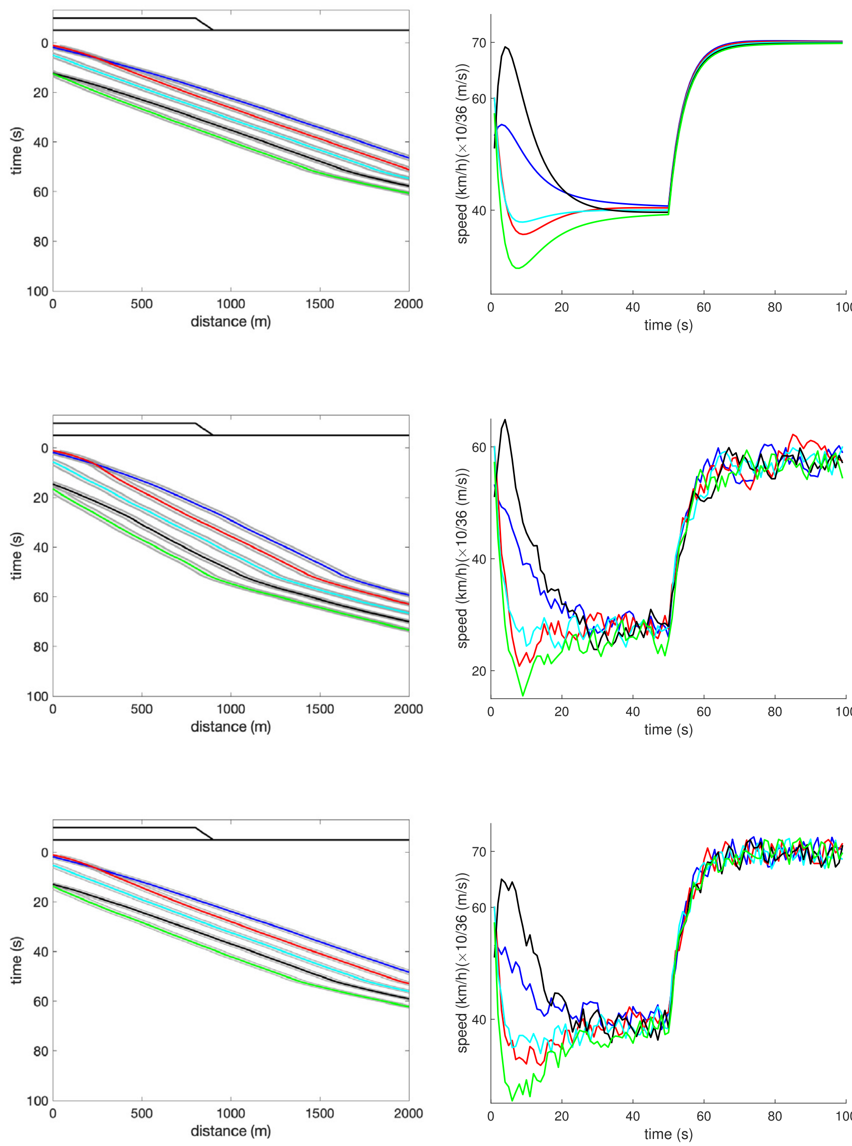

(c)

Fig. 7. Plot of distance and speed with (a) no disturbance, (b) disturbance, (c) disturbance and feedback. Consensus on the speed and distance of the train vehicles in the case of (a) no disturbance, (b) disturbance but no feedback control $\tilde{F}$, (c) disturbance and feedback control $\tilde{F}$ as in (20), where F_1 is defined in (25).

Appendix A

Proof of Theorem 1. The error dynamics can be written

$$\begin{bmatrix} \dot{\epsilon}_1 \\ \dot{\epsilon}_2 \end{bmatrix} \begin{bmatrix} \dot{\hat{x}}_1 - \dot{x}_1 \\ \dot{\hat{x}}_2 - \dot{x}_2 \end{bmatrix} = \begin{bmatrix} 0 & 1 \\ -\frac{k}{M} & -\frac{\tilde{k}}{M} \end{bmatrix} \begin{bmatrix} \epsilon_1 \\ \epsilon_2 \end{bmatrix} + \begin{bmatrix} 0 \\ \frac{a+bx_2+cx_2^2+f_2(.)}{M} \end{bmatrix} - \begin{bmatrix} 0 \\ \frac{F_1}{M} \end{bmatrix}.$$

Using control (14), the error dynamics above can be rewritten

$$\begin{bmatrix} \dot{\epsilon}_1 \\ \dot{\epsilon}_2 \end{bmatrix} = \begin{bmatrix} 0 & 1 \\ -\frac{k+\mu}{M} & -\frac{\tilde{k}+\tilde{\mu}}{M} \end{bmatrix} \begin{bmatrix} \epsilon_1 \\ \epsilon_2 \end{bmatrix} + \begin{bmatrix} 0 \\ \frac{f_1+f_2}{M} \end{bmatrix}. \tag{30}$$

Then the equilibrium point is obtained as

$$\begin{aligned} \begin{bmatrix} \epsilon_1^* \\ \epsilon_2^* \end{bmatrix} &= \lim_{t\to\infty} \begin{bmatrix} \hat{x}_1 - x_1 \\ \hat{x}_2 - x_2 \end{bmatrix} \\ &= \begin{bmatrix} -\frac{\tilde{k}+\tilde{\mu}}{k+\mu} & -\frac{M}{k+\mu} \\ 1 & 0 \end{bmatrix} \begin{bmatrix} 0 \\ -\frac{a+bx_2(t)+cx_2^2(t)+f_2(x_1,x_2,t)}{M} \end{bmatrix} \\ &= \begin{bmatrix} \frac{a+bx_2(t)+cx_2^2(t)+f_2(x_1,x_2,t)}{k+\mu} \\ 0 \end{bmatrix}. \end{aligned} \tag{31}$$

From $\lim_{t\to\infty} x_i^d$, $i = 1, 2$

$$\lim_{t\to\infty} \begin{bmatrix} \hat{x}_1 \\ \hat{x}_2 \end{bmatrix} = \begin{bmatrix} x_1^d \\ x_2^d \end{bmatrix}. \tag{32}$$

Then the following equation can be obtained

$$\lim_{t\to\infty}\begin{bmatrix} x_1 \\ x_2 \end{bmatrix} = \begin{bmatrix} x_1^d - \frac{a+bx_2(t)+cx_2^2(t)+f_2(x_1,x_2,t)}{k+\mu} \\ x_2^d \end{bmatrix}, \tag{33}$$

and this concludes the proof.

Proof of Theorem 2. For the first part, stability derives from $Tr(A) = -\frac{\tilde{k}}{M}$, where $Tr(A)$ is the trace of matrix A and from $\Delta(A) = \frac{k}{M} > 0$, where $\Delta(A)$ is the determinant of matrix A. Note that stability depends on the eigenvalues of A and that the expression of the eigenvalues is given by

$$\lambda_{1,2} = \frac{Tr(A)\pm\sqrt{Tr(A)^2-4\Delta(A)}}{2} = \frac{1}{2}\Big(-\frac{\tilde{k}}{M} \pm \sqrt{(\frac{\tilde{k}}{M})^2 - 4\frac{k}{M}}\Big). \tag{34}$$

As the trace $Tr(A)$ is strictly negative and the determinant $\Delta(A)$ is strictly positive, then it can be concluded that the system is stable.

As for the rest of the proof, it is known that if $\tilde{k} > 2\sqrt{kM}$ then $Tr(A)^2 > 4\Delta(A)$ and the origin is an asymptotically stable node. This corresponds to the case where the system is stable and no oscillations occur.

The last case is when $\tilde{k} < 2\sqrt{kM}$ which implies $Tr(A)^2 < 4\Delta(A)$ and therefore the origin is an asymptotically stable spiral. This corresponds to the case where the system is stable but oscillations may occur due to imaginary parts in the eigenvalues.

Proof of Lemma 1. Eq. (10) yields

$$\begin{aligned} &M\dot{v}_i(t) = k(p_{id}(t) - p_i(t)) + \tilde{k}(v_{id}(t) - v_i(t)) \\ &+\xi(v_{ref}(t) - v_i(t)) - f_1(v_i,t) - f_2(p_i,v_i,t), \end{aligned} \tag{35}$$

where $p_{id}(t)$ and $v_{id}(t)$ are the desired position and velocity of vehicle i. From $\sum_j \mu_{ij} = \sum_j \tilde{\mu}_{ij} = 1$, the above becomes $M\dot{v}_i(t) = k((\sum_j \mu_{ij}(p_j(t) - \Delta_{ji})) - p_i(t)) + \tilde{k}((\sum_j \tilde{\mu}_{ij} v_j(t)) - v_i(t)) + \xi(v_{ref}(t) - v_i(t)) - f_1(v_i,t) - f_2(p_i,v_i,t)$, where $\Delta_{ji} := \delta_i - \delta_j$. From the definition above of $k_{ij} := k\mu_{ij}$, and $\tilde{k}_{ij} := \tilde{k}\tilde{\mu}_{ij}$, Eq. (35) can be rearranged as $M\dot{v}_i(t) = \sum_j k_{ij}(p_j(t) - \delta_j + \delta_i - p_i(t)) + \sum_j \tilde{k}_{ij}(v_j(t) - v_i(t)) + \xi(v_{ref}(t) - v_i(t)) - f_1(v_i,t) - f_2(p_i,v_i,t)$, which concludes the proof.

Proof of Theorem 3. This proof builds on the analysis of the dynamics for the error defined in (24), which for general F_1 is given by

$$\begin{bmatrix} \dot{E}_1 \\ \dot{E}_2 \end{bmatrix} = \begin{bmatrix} 0 & 1 \\ -L & -\tilde{L} \end{bmatrix}\begin{bmatrix} E_1 \\ E_2 \end{bmatrix} + \begin{bmatrix} 0 \\ \left[\frac{f_{12}^i - \xi e_2^i(t) - F_1^i}{M_i}\right]_{i\in V} \end{bmatrix},$$

where $E_j = [e_j^i]_{i\in V}$. Under control (25), for the above error dynamics the following system can be obtained

$$\begin{bmatrix} \dot{E}_1 \\ \dot{E}_2 \end{bmatrix} = \underbrace{\begin{bmatrix} 0 & 1 \\ -L - diag(\frac{\mu}{M_i}) & -\tilde{L} - diag(\frac{\xi+\tilde{\mu}}{M_i}) \end{bmatrix}}_{\mathcal{A}}\begin{bmatrix} E_1 \\ E_2 \end{bmatrix} + \Delta(X_1, X_2).$$

At the equilibrium, the following equation holds true: $\begin{bmatrix} (E_1^*)^T & (E_2^*)^T \end{bmatrix}^T = -\mathcal{A}^{-1}\Delta(X_1, X_2)$. From (23) and the above equation, Eq. (26) can be obtained and this concludes the proof.

Proof of Theorem 4. Solve for $det(\lambda\mathbb{I} - \mathcal{A}) = 0$ and find the roots of such set of equation. To this aim, note that for a given generic block matrix, the following equation holds

$$det(\begin{bmatrix} A & B \\ C & D \end{bmatrix}) = det(AD - CB), \quad \text{if } AC = CA. \tag{36}$$

Hence,

$$det(\lambda\mathbb{I} - \mathcal{A}) = det\left(\begin{bmatrix} \lambda\mathbb{I} & -\mathbb{I} \\ L + diag\left(\frac{\mu_i}{M_i}\right) & \lambda\mathbb{I} + \tilde{L} + diag\left(\frac{\xi+\tilde{\mu}}{M_i}\right) \end{bmatrix}\right). \tag{37}$$

Then it can be concluded that $det(\lambda^2\mathbb{I} + \lambda\mathbb{I}\cdot L + \lambda\mathbb{I}\cdot diag(\frac{\xi+\tilde{\mu}}{M_i}) + L + diag(\frac{\mu}{M_i}))$.

Without loss of generality, the assumption that $L = \tilde{L}$ is used to obtain the second equality. Actually, if $\tilde{L}$ is a scaled version of L, the methodology is still valid, but a scaling factor needs to be introduced in the equation below. Under the assumption that the mass of the trains are similar, namely $M_i \approx M$ for all i, the following equations can be obtained

$$\begin{aligned} &det(\lambda^2\mathbb{I} + \lambda\mathbb{I}\cdot L + \lambda\mathbb{I}\cdot diag(\tfrac{\xi+\tilde{\mu}}{M}) + L + diag(\tfrac{\mu}{M})) \\ &= det\Big((\lambda^2 + \lambda\tfrac{\xi+\tilde{\mu}}{M} + \tfrac{\mu}{M})\mathbb{I} + (\lambda+1)L\Big) \\ &= \textstyle\prod_{i=1}^n\Big((\lambda^2 + \lambda\tfrac{\xi+\tilde{\mu}}{M} + \tfrac{\mu}{M}) - (\lambda+1)\eta_i\Big) = 0, \end{aligned} \tag{38}$$

the ith eigenvalue of $-L$ is denoted by η_i. To obtain the roots of the set of Eqs. (38) the equation $\lambda^2 + \lambda(\frac{\xi+\tilde{\mu}}{M} - \eta_i) + \frac{\mu}{M} - \eta_i = 0$ needs to be solved. By doing this, the roots are obtained as

$$\begin{aligned} \lambda_i^+ &= \frac{-(\frac{\xi+\tilde{\mu}}{M} - \eta_i) + \sqrt{(\frac{\xi+\tilde{\mu}}{M} - \eta_i)^2 - 4(\frac{\mu}{M} - \eta_i)}}{2}, \\ \lambda_i^- &= \frac{-(\frac{\xi+\tilde{\mu}}{M} - \eta_i) - \sqrt{(\frac{\xi+\tilde{\mu}}{M} - \eta_i)^2 - 4(\frac{\mu}{M} - \eta_i)}}{2}. \end{aligned} \tag{39}$$

From the above equations, after noting that the real part of the eigenvalues is negative, it can be concluded that the equilibrium point (26) is asymptotically stable.

For the second part, note that if $\frac{\xi+\tilde{\mu}}{M} - \eta_i > \sqrt{4\frac{\mu}{M} - \eta_i}$ then both eigenvalues in (39) have no imaginary parts, and therefore the equilibrium point (26) is an asymptotically stable node. On the contrary, if $\frac{\xi+\tilde{\mu}}{M} - \eta_i < \sqrt{4\frac{\mu}{M} - \eta_i}$ both eigenvalues in (39) are complex imaginary and consequently the equilibrium point (26) is an asymptotically stable spiral.

Proof of Corollary 1. Note that the determinant is positive if $(\frac{\xi+\tilde{\mu}}{M} - \eta_i)^2 - 4(\frac{\mu}{M} - \eta_i) > 0$. From the above inequality it can be obtained $(\frac{\xi+\tilde{\mu}}{M})^2 + (\eta_i)^2 - 2(\frac{\tilde{k}+\tilde{\mu}}{M})(\eta_i) - 4(\frac{\mu}{M} - \eta_i) > 0$, which yields

$$\tilde{\phi}(\eta_i) := (\eta_i)^2 + [4 - 2(\frac{\xi+\tilde{\mu}}{M})]\eta_i > -(\frac{\xi+\tilde{\mu}}{M})^2 + 4\frac{\mu}{M}. \tag{40}$$

The LHS attains a minimum for $\eta_i^* = -[2 - (\frac{\xi+\tilde{\mu}}{M})]$ and the minimum is $\tilde{\phi}(\eta_i^*) = -[2 - (\frac{\xi+\tilde{\mu}}{M})]^2$. A sufficient condition for (40) to hold is that $\tilde{\phi}(\eta_i^*) = -[2 - (\frac{\xi+\tilde{\mu}}{M})]^2 > -(\frac{\xi+\tilde{\mu}}{M})^2 + 4\frac{\mu}{M}$. Expanding the LHS the above can be rewritten as $-1 + (\frac{\xi+\tilde{\mu}}{M}) > \frac{\mu}{M}$, from which the following relation between the feedback control parameters ξ, μ and $\tilde{\mu}$ is obtained: $-M + \xi + \tilde{\mu} > \mu$. This ends the proof.

References

Bauso, D., Giarré, L., & Pesenti, R. (2006). Mechanism design for optimal consensus problems. In *Proceedings of the 45th IEEE conference on decision and control* (pp. 3381–3386). IEEE.

Bersani, C., Qiu, S., Sacile, R., Sallak, M., & Schön, W. (2015). Rapid, robust, distributed evaluation and control of train scheduling on a single line track. *Control Engineering Practice*, *35*, 12–21.

Corman, F., D'Ariano, A., Pacciarelli, D., & Pranzo, M. (2010). A tabu search algorithm for rerouting trains during rail operations. *Transportation Research, Part B (Methodological)*, *44*(1), 175–192.

D'ariano, A., Pacciarelli, D., & Pranzo, M. (2007). A branch and bound algorithm for scheduling trains in a railway network. *European Journal of Operational Research*, *183*(2), 643–657.

D'Ariano, A., Pranzo, M., & Hansen, I. A. (2007). Conflict resolution and train speed coordination for solving real-time timetable perturbations. *IEEE Transactions on Intelligent Transportation Systems*, *8*(2), 208–222.

Dong, H., Gao, S., & Ning, B. (2016). Cooperative control synthesis and stability analysis of multiple trains under moving signaling systems. *IEEE Transactions on Intelligent Transportation Systems*, *17*(10), 2730–2738.

Dunbar, W. B., & Murray, R. M. (2006). Distributed receding horizon control for multi-vehicle formation stabilization. *Automatica*, *42*(4), 549–558.

Fax, J. A., & Murray, R. M. (2004). Information flow and cooperative control of vehicle formations. *IEEE Transactions on Automatic Control*, *49*(9), 1465–1476.

Felez, J., Kim, Y., & Borrelli, F. (2019). A model predictive control approach for virtual coupling in railways. *IEEE Transactions on Intelligent Transportation Systems*, *20*(7), 2728–2739.

Friedrich, J., Restel, F. J., & Wolniewicz, Ł. (2018). Railway operation schedule evaluation with respect to the system robustness. In *International conference on dependability and complex systems* (pp. 195–208). Springer.

Gao, K., Huang, Z., Wang, J., Peng, J., & Liu, W. (2013). Decentralized control of heavy-haul trains with input constraints and communication delays. *Control Engineering Practice*, *21*(4), 420–427.

Giulietti, F., Pollini, L., & Innocenti, M. (2000). Autonomous formation flight. *IEEE Control Systems Magazine*, *20*(6), 34–44.

Hansen, H. S., Nawaz, M. U., & Olsson, N. (2017). Using operational data to estimate the running resistance of trains. estimation of the resistance in a set of norwegian tunnels. *Journal of Rail Transport Planning & Management*, *7*(1–2), 62–76.

Iwnicki, S. (2006). *Handbook of railway vehicle dynamics*. CRC Press.

Jadbabaie, A., Lin, J., & Morse, A. S. (2003). Coordination of groups of mobile autonomous agents using nearest neighbor rules. *IEEE Transactions on Automatic Control*, *48*(6), 988–1001.

Jiao, J., Zhang, F., & Liu, J. (2020). A spatiotemporal analysis of the robustness of high-speed rail network in China. *Transportation Research Part D: Transport and Environment*, *89*, Article 102584.

Liu, Y., & Passino, K. M. (2004). Stable social foraging swarms in a noisy environment. *IEEE Transactions on Automatic Control*, *49*(1), 30–44.

Lusby, R. M., Larsen, J., & Bull, S. (2018). A survey on robustness in railway planning. *European Journal of Operational Research*, *266*(1), 1–15.

Ning, B., Xun, J., Gao, S., & Zhang, L. (2014). An integrated control model for headway regulation and energy saving in urban rail transit. *IEEE Transactions on Intelligent Transportation Systems*, *16*(3), 1469–1478.

Olfati-Saber, R., Fax, J. A., & Murray, R. M. (2007). Consensus and cooperation in networked multi-agent systems. *Proceedings of the IEEE*, *95*(1), 215–233.

Olfati-Saber, R., & Murray, R. M. (2004). Consensus problems in networks of agents with switching topology and time-delays. *IEEE Transactions on Automatic Control*, *49*(9), 1520–1533.

Ren, W. (2007). Consensus strategies for cooperative control of vehicle formations. *IET Control Theory & Applications*, *1*(2), 505–512.

Ren, W., & Beard, R. W. (2005). Consensus seeking in multiagent systems under dynamically changing interaction topologies. *IEEE Transactions on Automatic Control*, *50*(5), 655–661.

Ren, W., Beard, R. W., & Atkins, E. M. (2005). A survey of consensus problems in multi-agent coordination. In *Proceedings of the 2005, American control conference, 2005* (pp. 1859–1864). IEEE.

Santini, S., Salvi, A., Valente, A. S., Pescapé, A., Segata, M., & Cigno, R. L. (2016). A consensus-based approach for platooning with intervehicular communications and its validation in realistic scenarios. *IEEE Transactions on Vehicular Technology*, *66*(3), 1985–1999.

Shamma, J. (2008). *Cooperative control of distributed multi-agent systems*. John Wiley & Sons.

Su, S., Wang, X., Tang, T., Wang, G., & Cao, Y. (2021). Energy-efficient operation by cooperative control among trains: A multi-agent reinforcement learning approach. *Control Engineering Practice*, *116*, Article 104901.

Wang, H., Yu, F. R., Zhu, L., Tang, T., & Ning, B. (2015). A cognitive control approach to communication-based train control systems. *IEEE Transactions on Intelligent Transportation Systems*, *16*(4), 1676–1689.

Wu, Q., Spiryagin, M., & Cole, C. (2016). Longitudinal train dynamics: an overview. *Vehicle System Dynamics*, *54*(12), 1688–1714.

Xun, J., Ning, B., Tang, T., & Dong, H. (2013). Cooperative control for train headway adjustment in railway traffic. *IFAC Proceedings Volumes*, *46*(25), 1–6.

Xun, J., Yin, J., Liu, R., Liu, F., Zhou, Y., & Tang, T. (2019). Cooperative control of high-speed trains for headway regulation: A self-triggered model predictive control based approach. *Transportation Research Part C (Emerging Technologies)*, *102*, 106–120.

Yin, H., Mehta, P. G., Meyn, S. P., & Shanbhag, U. V. (2011). Synchronization of coupled oscillators is a game. *IEEE Transactions on Automatic Control*, *57*(4), 920–935.

Yin, H., Mehta, P. G., Meyn, S. P., & Shanbhag, U. V. (2014). On the efficiency of equilibria in mean-field oscillator games. *Dynamic Games and Applications*, *4*(2), 177–207.

Yin, J., Tang, T., Yang, L., Xun, J., Huang, Y., & Gao, Z. (2017). Research and development of automatic train operation for railway transportation systems: A survey. *Transportation Research Part C (Emerging Technologies)*, *85*, 548–572.

Zhu, L., Yu, F. R., Ning, B., & Tang, T. (2014). Design and performance enhancements in communication-based train control systems with coordinated multipoint transmission and reception. *IEEE Transactions on Intelligent Transportation Systems*, *15*(3), 1258–1272.